Supporting Information for

Single-crystal elasticity of phase Egg $AlSiO_3OH$ and δ-AlOOH by Brillouin spectroscopy

Baoyun Wang[1,2,3], Yanyao Zhang[3], Suyu Fu[3,4], Wei Yan[5,6], Eiichi Takahashi[1,7], Li Li[1,7], Jung-Fu Lin [3*], Maoshuang Song[1,7*]

[1]State Key Laboratory of Isotope Geochemistry, Guangzhou Institute of Geochemistry, Chinese Academy of Sciences, Guangzhou 510640, China;

[2]College of Earth and Planetary Sciences, University of Chinese Academy of Sciences, Beijing, 100049, China;

[3]Department of Geological Sciences, Jackson School of Geosciences, The University of Texas at Austin, Austin, 78712 Texas, USA;

[4]School of Earth and Space Exploration, Arizona State University

[5]School of Earth and Space Sciences, Peking University, Beijing, 100871, China

[6]Key Laboratory of Orogenic Belts and Crustal Evolution, Ministry of Education of China, Beijing, 100871, China

[7]CAS Center for Excellence in Deep Earth Science, Guangzhou, 510640, China

[*]Corresponding email: afu@jsg.utexas.edu; msong@gig.ac.cn

Contents of this file

Table OM1. Electron microprobe data (wt% of oxides) of phase Egg and δ-AlOOH.

	Phase Egg					δ-AlOOH				
	Position 1	Position 2	Position 3	Position 4	Average	Position 1	Position 2	Position 3	Position 4	Average
Na_2O	-	-	-	-	-	0.01	-	0.02	0.02	0.02
FeO	0.06	-	0.02	-	0.04	0.01	0.01	-	0.17	0.06
K_2O	-	-	-	-	-	-	-	-	-	-
SiO_2	50.29	50.40	50.71	50.80	50.55	0.06	0.08	0.08	0.10	0.08
Cr_2O_3	-	-	0.01	-	0.01	0.01	0.02	0.01	0.01	0.01
CaO	0.02	-	0.01	0.02	0.01	-	-	-	-	-
Al_2O_3	41.86	41.68	41.44	41.93	41.72	84.83	85.11	84.35	84.28	84.64
MgO	-	-	-	-	-	-	-	-	-	-
H_2O[a]	7.77	7.91	7.81	7.25	7.69	15.08	14.78	15.55	15.43	15.21

[a] H_2O was calculated from the weight deficiency in total.

Table OM2. Elastic properties of typical mantle minerals under ambient conditions.

Mineral	Composition	ρ(g/cm^3)	K_S (GPa)	G (GPa)	V_P (km/s)	V_S (km/s)	AV_P	AV_S	Reference
Olivine	$(Mg_{0.9}Fe_{0.1})_2SiO_4$	3.343	129.6	77.8	8.35	4.82	24.3	18.0	Mao et al. (2015)
Enstatite	$(Mg_{1.74}Fe_{0.16}Al_{0.05}Ca_{0.04}Cr_{0.02})(Si_{1.94}Al_{0.06})O_6$	3.288	112.5	75.9	8.06	4.80	14.0	13.7	Zhang and Bass (2016)
Diopside	$Ca_{0.99}Mg_{0.79}Fe_{0.21}Si_{2.01}O_6$	3.345	117.0	70.0	7.92	4.57	25.9	21.2	Fan et al. (2020)
Wadsleyite	$(Mg_{0.915}Fe_{0.075})_2SiO_4$	3.570	170.1	108.0	9.38	5.50	19.0	17.5	Wang et al. (2014)
Hydrous wadsleyite	0.84 wt.% H_2O	3.435	160.4	105.4	9.36	5.54	15.8	15.6	Mao et al. (2008)
Ringwoodite	$(Mg_{0.91}Fe_{0.09})_2SiO_4$	3.701	188.3	119.6	9.69	5.68	4.7	10.3	Sinogeikin et al. (1998)
Hydrous ringwoodite	$(Mg_{1.633}Fe^{2+}_{0.231}Fe^{3+}_{0.026})\ Si_{1.00}H_{0.179}O_4$	3.649	175.0	106.0	9.31	5.39	4.6	10.4	Mao et al. (2012)
Majorite	$(Ca_{0.39}\ Mg_{2.66})((Mg,Si)_{0.84}Al_{1.14})Si_3O_{12}$	3.460	159.0	87.1	8.92	5.02	0.3	0.7	Sanchez-Valle et al. (2019)
Pyrope	$Mg_{3.006}Al_{1.995}Si_{3.005}O_{12}$ (900 ppm H_2O)	3.557	168.6	92.3	9.05	5.09	0.9	2.1	Fan et al. (2019)
Bridgmanite	$MgSiO_3$	4.106	253.6	175.0	10.89	6.53	7.6	15.4	Sinogeikin et al. (2004)
Ferropericlase	$Mg_{0.94}Fe_{0.06}O$	3.723	163.3	121.0	9.34	5.70	11.7	23.9	Jackson et al. (2006)
Stishovite	SiO_2	4.301	308.2	228.1	11.93	7.28	25.6	34.2	Jiang et al. (2009)
Phase Egg	$Al_{0.981}Si_{1.008}O_4H_{1.022}$	3.740	158.3	123.0	9.28	5.73	38.4	22.1	this study
δ-AlOOH	AlOOH	3.536	162.9	145.2	10.04	6.41	19.1	12.7	this study

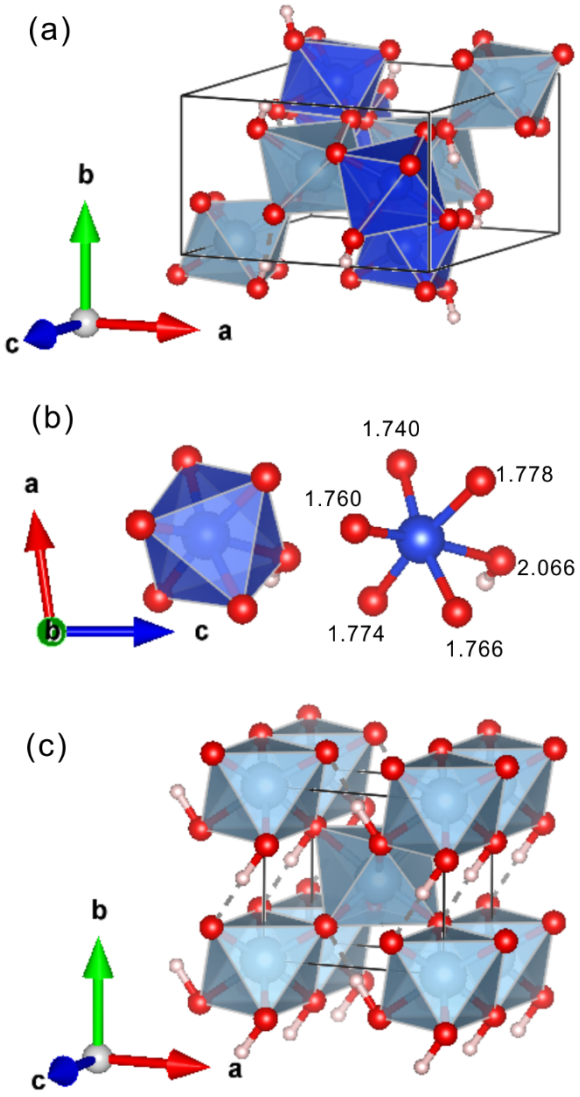

Figure OM1. (a) The structure of phase Egg. (b) The SiO_6 octahedron in phase Egg and the length of Si-O bonds (unit: Å) are shown (Schmidt et al. 1998). (c) The structure of δ-AlOOH. The Al, Si and O atoms are shown in gray, blue and red, respectively. The H atoms are small white spheres. The images were drawn using VESTA software (Momma and Izumi 2008).

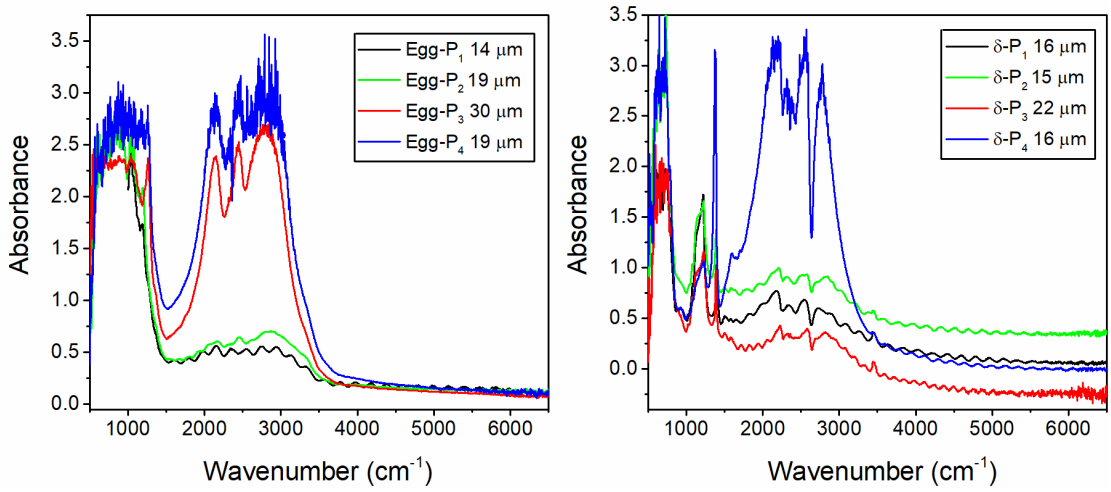

Figure OM2. Unpolarized FTIR spectra of single-crystal phase Egg and δ-AlOOH. (a) phase Egg. (b) δ-AlOOH. Four platelets (P_1 to P_4) with random crystallographic orientations were used in this study for each phase. Crystal thicknesses are labelled in micrometer (μm).

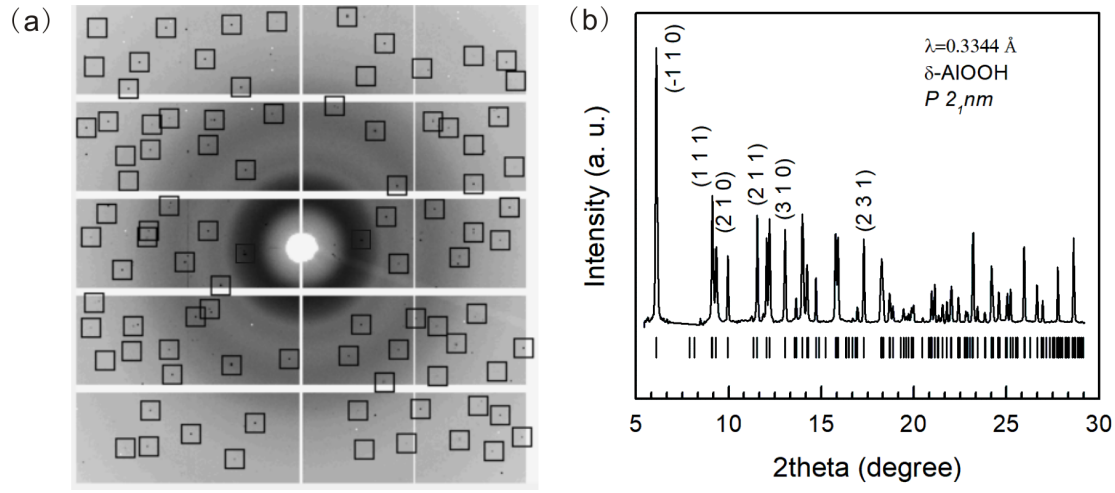

Figure OM3. X-ray diffraction results of δ-AlOOH at ambient conditions. (a) is the raw CCD image and (b) is the integrated pattern. Miller indexes are labelled next to major diffraction peaks. The short vertical lines represent simulated diffraction peak positions of δ-AlOOH.

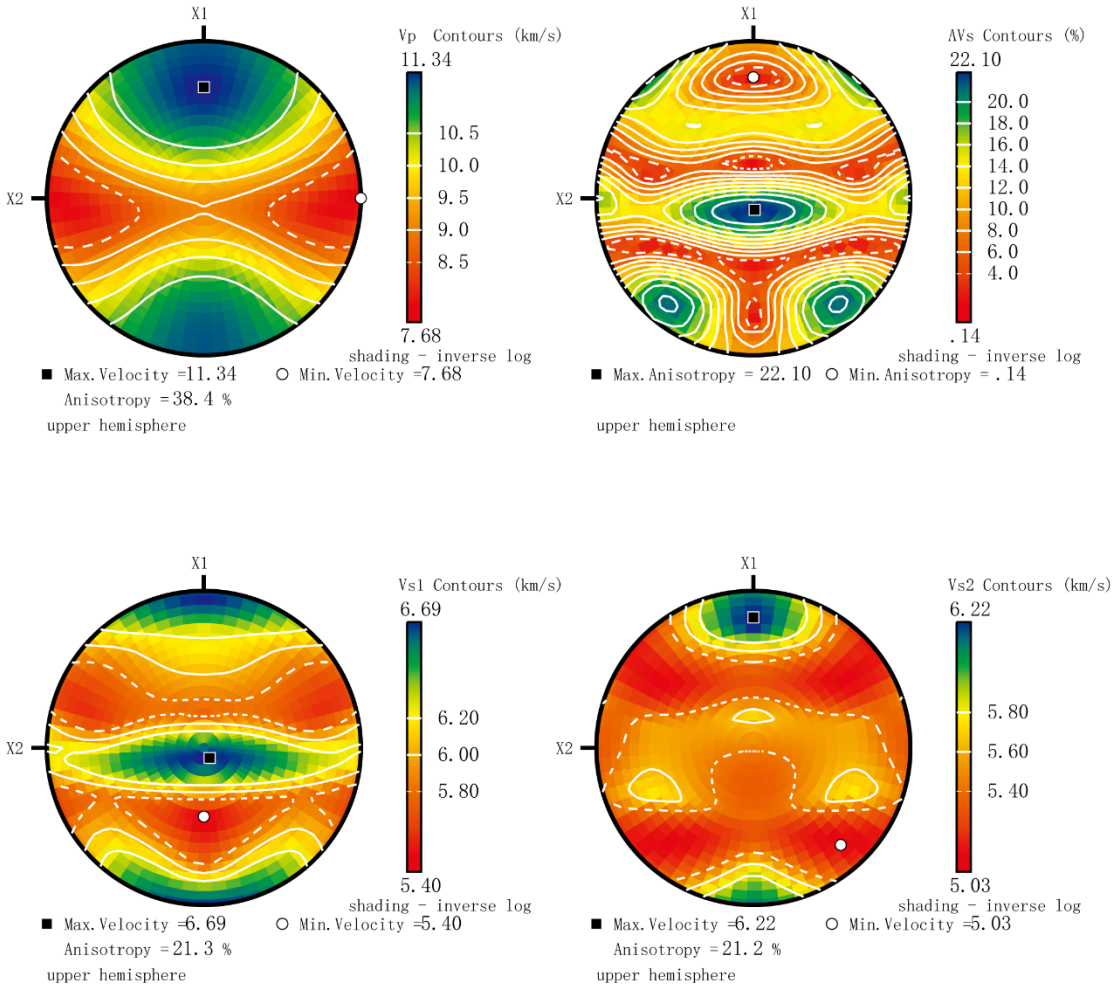

Figure OM4. Upper hemisphere pole figures of the compressional wave (V_P), shear wave (V_{S1}, V_{S2}) and shear-wave splitting (V_S) anisotropy of phase Egg. The figure was drawn using the UNICEF Careware software (Mainprice 1990).

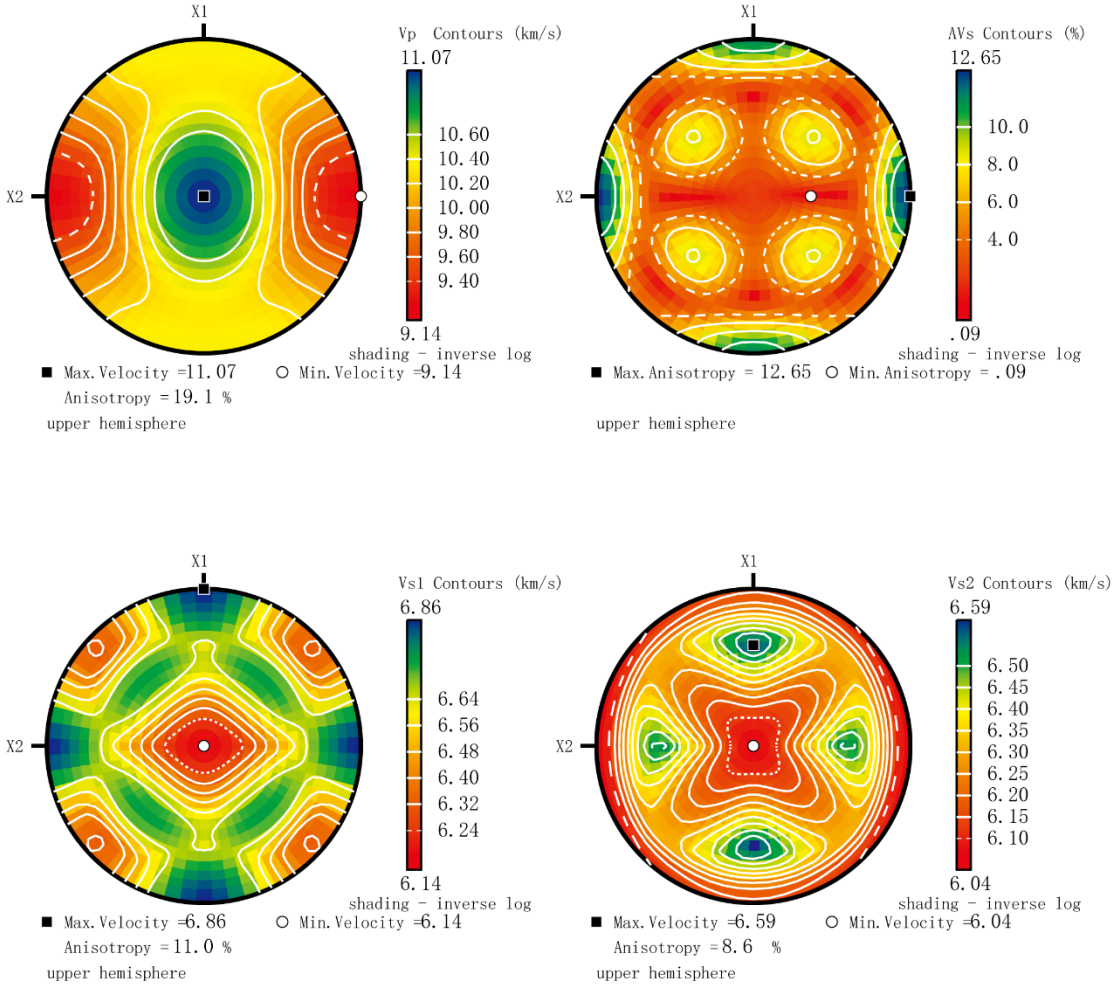

Figure OM5. Upper hemisphere pole figures of the compressional wave (V_P), shear wave (V_{S1}, V_{S2}) and shear-wave splitting (V_S) anisotropy of δ-AlOOH. The figure was drawn using the UNICEF Careware software (Mainprice 1990).

References cited

Fan, D., Fu, S., Lu, C., Xu, J., Zhang, Y., Tkachev, S.N., Prakapenka, V.B., and Lin, J.-F. (2020) Elasticity of single-crystal Fe-enriched diopside at high-pressure conditions: Implications for the origin of upper mantle low-velocity zones. American Mineralogist: Journal of Earth and Planetary Materials, 105(3), 363-374.

Fan, D., Xu, J., Lu, C., Tkachev, S.N., Li, B., Ye, Z., Huang, S., Prakapenka, V.B., and Zhou, W. (2019) Elasticity of single-crystal low water content hydrous pyrope at high-pressure and high-temperature conditions. American Mineralogist: Journal of Earth and Planetary Materials, 104(7), 1022-1031.

Jackson, J.M., Sinogeikin, S.V., Jacobsen, S.D., Reichmann, H.J., Mackwell, S.J., and Bass, J.D. (2006) Single‐crystal elasticity and sound velocities of $(Mg_{0.94}Fe_{0.06})O$ ferropericlase to 20 GPa. Journal of Geophysical Research: Solid Earth, 111(B9).

Jiang, F., Gwanmesia, G.D., Dyuzheva, T.I., and Duffy, T.S. (2009) Elasticity of stishovite and acoustic mode softening under high pressure by Brillouin scattering. Physics of the Earth and Planetary Interiors, 172(3-4), 235-240.

Mainprice, D. (1990) A Fortran program to calculate seismic anisotropy from the lattice preferred orientation of minerals. Computers & Geosciences, 16(3), 385–393

Mao, Z., Fan, D., Lin, J.-F., Yang, J., Tkachev, S.N., Zhuravlev, K., and Prakapenka, V.B. (2015) Elasticity of single-crystal olivine at high pressures and temperatures. Earth and Planetary Science Letters, 426, 204-215.

Mao, Z., Jacobsen, S., Jiang, F., Smyth, J., Holl, C., and Duffy, T. (2008) Elasticity of hydrous wadsleyite to 12 GPa: implications for Earth's transition zone. Geophysical Research Letters, 35(21).

Mao, Z., Lin, J.-F., Jacobsen, S.D., Duffy, T.S., Chang, Y.-Y., Smyth, J.R., Frost, D.J.,

Hauri, E.H., and Prakapenka, V.B. (2012) Sound velocities of hydrous ringwoodite to 16 GPa and 673 K. Earth and Planetary Science Letters, 331, 112-119.

Momma, K., and Izumi, F. (2008) VESTA: a three-dimensional visualization system for electronic and structural analysis. Journal of Applied Crystallography, 41(3), 653-658.

Sanchez-Valle, C., Wang, J., and Rohrbach, A. (2019) Effect of calcium on the elasticity of majoritic garnets and the seismic gradients in the mantle transition zone. Physics of the Earth and Planetary Interiors, 293, 106272.

Schmidt, M.W., Finger, L.W., Angel, R.J., and Dinnebier, R.E. (1998) Synthesis, crystal structure, and phase relations of $AlSiO_3OH$, a high-pressure hydrous phase. American Mineralogist, 83(7-8), 881-888.

Sinogeikin, S., Katsura, T., and Bass, J.D. (1998) Sound velocities and elastic properties of Fe‐bearing wadsleyite and ringwoodite. Journal of Geophysical Research: Solid Earth, 103(B9), 20819-20825.

Sinogeikin, S.V., Zhang, J., and Bass, J.D. (2004) Elasticity of single crystal and polycrystalline $MgSiO_3$ perovskite by Brillouin spectroscopy. Geophysical Research Letters, 31(6).

Wang, J., Bass, J.D., and Kastura, T. (2014) Elastic properties of iron-bearing wadsleyite to 17.7 GPa: Implications for mantle mineral models. Physics of the Earth and Planetary Interiors, 228, 92-96.

Zhang, J.S., and Bass, J.D. (2016) Single‐crystal elasticity of natural Fe‐bearing orthoenstatite across a high‐pressure phase transition. Geophysical Research Letters, 43(16), 8473-8481.